

# CFD Investigation of Complex Phenomena in S-Shape Region of Reversible Pump-Turbine

C Jacquet<sup>1</sup>, R Fortes-Patella<sup>1</sup>, L Balarac<sup>2</sup>, J-B Houdeline<sup>2</sup>

<sup>1</sup> SuperGrid Institute, 130 rue Léon Blum, 69611 Villeurbanne, France

<sup>2</sup> GE Renewable Energy, 82, Avenue Léon Blum, 38041 Grenoble, France

clement.jacquet@ge.com

**Abstract.** Pumped Storage Plants (PSP) using reversible pump-turbines offer the possibility to store large amounts of energy with high efficiency and at reasonable cost. For reversible high head pump-turbines, the characteristic curves exhibit an S-shape in the turbine, turbine break and reverse pump quadrants. This S-shape leads to unstable behaviour of the turbine when coupling to the grid (for small guide vane opening) or to surge transient phenomena in case of emergency shutdown (for large guide vane opening). Typically the piping system can be exposed to severe pressure oscillations. Furthermore, the flow inside the pump-turbine is characterized by unsteady complex hydrodynamic phenomena. These phenomena have to be deeply investigated to improve the behaviour of the pump-turbine in such operating conditions. This paper focuses on the numerical analysis of the flow in a reversible pump-turbine in the S-shape region. For this application, we used unsteady computation applying the SAS-SST turbulence model and considered a full computational domain that includes all the component of the pump-turbine. The study highlights the evolution of the flow behaviour for a large range of operating conditions: from the optimal efficiency point to the zero discharge condition, for a given constant guide vane opening.

## 1. Introduction

Today, the part of the renewable energy source in the electricity production expands rapidly. And it is expected to become more and more important during the next decade. Intermittency of the energy sources increases the need for regulation in a system where production must equals consumption at all time. Pumped Storage Plants using reversible pump-turbines are often looked at as one of the most economically viable way to provide stability to the electricity grid. Although, the existing technology of pump-turbines needs to be adapted in order to respond this new need. One of the most important challenge is to improve start-up and shutdown procedures. Pump-turbines, and especially high head pump-turbine, have characteristics curves that exhibit an S-Shape in turbine, turbine break and reverse-pump quadrant. This S-shape can lead system to oscillations when coupling with the grid [1], and also to severe pressure surge in the piping system during emergency shutdown [2], [3]. A lot of information can be found in literature about the hydraulic origin of the S-Shape for small guide-vane openings and about how to address the coupling issues [4]–[6]. Whereas very few is available about the flow patterns inside pump-turbines operating in the “S” region for large guide vane opening.

The aim of the work presented in this paper is to perform a comprehensive numerical analysis of the flow behaviour inside a pump-turbine operating for 5 relevant operating points, for a large guide vane opening. The first step is the setup and the validation of the numerical model by comparing with the available experimental results. The calculated pressure pulsations is then analysed to determine the



main sources of instability. Finally, description of the flow pattern for all considered operating points is detailed.

## 2. Methodology

### 2.1. Studied configuration

**2.1.1. Pump-turbine geometry.** One pump-turbine geometry designed by General Electric is considered for the numerical simulations. The runner has a specific speed ( $n_q$ ) of approximately 40. With  $n_q$  defined as follows:

$$n_q = \frac{nQ^{1/2}}{H^{3/4}} \sim 40 \quad (1)$$

Where  $n$  is the rotation speed of the runner (*rpm*),  $H$  is the nominal head (*m*), and  $Q$  is the nominal discharge (*m<sup>3</sup>/s*).

The static parts of pump-turbine consist in a spiral casing (SC) including 20 stay vanes (SV), 20 guide vanes (GV) and a draft tube (DT). The rotating part is a nine-blade runner. Experimental results available for this configuration are used for the validation of the numerical model.

**2.1.2. List of operating points** In order to study the evolution of the flow pattern, a total of five operating points (*OP#*) are considered. The first operating point (*OP#1*) is located in the continuous operating range of the pump-turbine. The discharge is elevated (high load), and the pump-turbine operates with high efficiency. The second operating point (*OP#2*) is located at the change of the slope within the  $\Psi(\phi)$  graph. The third and fourth operating points are close to runaway condition (zero torque, no-load). The torque for *OP#3* is slightly positive; while *OP#4* is located in the turbine brake region. The discharge for *OP#5* approaches zero flow-rate condition. Guide vane opening is the same for all the considered operating points.

### 2.2. Computational methodology

**2.2.1. Computational domain and mesh.** **Table 1.** summarizes the principal mesh characteristics.

**Table 1** - Mesh characteristics

Subdomain	Mesh Type	Number of Nodes (million)	$y_+$	
			Mean	Max
SC	Hybrid	6.3	4	27
SV+ GV	Structured	11.2	13	29
Runner	Structured	5.8	12	44
DT	Structured	2.6	7	34
Full Domain	Hybrid	26	9	44

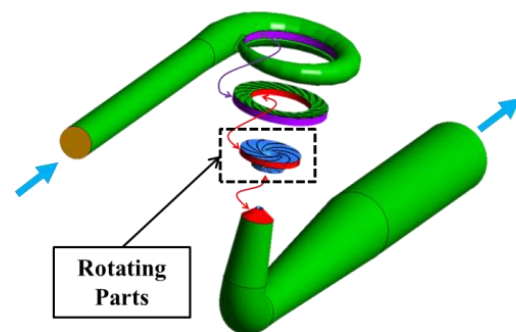


**Figure 1.** Computational Domain

Scale for the simulations is the same as the one for the model tests measurements (in GE laboratory). The numerical domain includes every component of the pump-turbine and is divided into four subdomains: the spiral casing, the stay vanes and guide vanes the runner, and the draft tube. The

runner tip (end of the runner hub) is included into the draft tube domain and considered as a rotating wall. Extensions are added both at the upstream and downstream sides, in order to limit the influence of the inlet and outlet boundary conditions. The clearance gaps between the rotor and stator components of the pump-turbine are not taken into account by the numerical model. Hybrid mesh is used for the spiral casing, and structured meshes are employed for the other components.

**2.2.2. Turbulence model** Numerical simulations are performed using the commercial software ANSYS CFX. Turbulence is modelled using the *SAS – SST* turbulence model, developed by Menter et al. [7]. This two-equation model includes an additional source term in the  $\omega$  equation, introducing a second length scale for the turbulent field. This Von Karman length scale is representative of the smallest instabilities (eddies) that can be resolved and depends on the spatial and time discretisation, as well as on the flow instabilities. Thus the eddy viscosity is automatically reduced in regions of the domain where instabilities are detected; the flow becomes unsteady and part of the turbulent spectrum is resolved. In region with no strong instability the model is equivalent to the well known *k –  $\omega$  SST* turbulence model.

**2.2.3. Numerical schemes.** Numerical scheme is set following the recommendations made in [8] for the use of SAS-SST turbulence model. Second order backward Euler scheme is used for time integration. Advection term in the momentum equation is discretized using a Second Order Upwind (SOU) scheme in the stable region of the flow. And a Central Difference (CD) scheme is employed in the region where SAS model is activated. The switch between SOU and CD is ensured by the use of a blending function. Regarding the equations for the turbulence quantities, discretization of the convection term is carried on by a first order upwind scheme.

Time step for the simulations corresponds to two degrees of the runner rotation.

**2.2.4. Boundary and initial conditions.** For the simulations, rotation of the runner is taken into account using the multiple frame of reference model (MFR). With MFR the solver uses two distinct sets of equations for the rotating and the stationary parts of the domain. Connexion between the different parts is ensured by the means of interfaces. Rotational speed of the runner is set to a constant value. Mass flow is specified at the inlet of the domain with normal direction to the boundary. Turbulent quantities at the inlet are specified using turbulence intensity ( $I_t = (3/2) \sqrt{k}/U_{inlet}$ ) and the turbulent length scale ( $L_t = \sqrt{k}/(C\mu^{0.25} \cdot \omega)$ ). In the previous expressions,  $k$  stands for the Turbulence kinetic energy ( $m^2/s^2$ ),  $U_{inlet}$  is the velocity at the inlet ( $m/s$ ), and  $\omega$  is the dissipation rate for  $k$  ( $s^{-1}$ ). Special attention is paid to the choice of the value for  $I_t$  and  $L_t$  in order to ensure proper development of the boundary layer in the upstream extension. Average static pressure boundary condition is used at the outlet of the domain. No slip wall with Automatic Wall Functions boundary condition is set for all the solid walls of the domain. Interfaces between rotating and static domains are treated with the “Transient Rotor Stator” model available in ANSYS CFX.

Initial solution fields for *OP#1* are provided by a steady state computation result. For *OP#2* initial condition is specified using the converged result of *OP#1*, and so on.

### 3. Results and discussions

#### 3.1. Validation of the numerical model

The discharge through the pump-turbine and its rotation speed are given as input parameters for the simulations. The two main results are thus the Head ( $H$  difference of total pressure between the SC inlet and DT outlet, expressed in meter) and the Torque ( $C$  in  $N.m$ ) exerted by the fluid on the runner. Static values for the head and torque are obtained by averaging the instantaneous values over at least 15 converged runner revolutions. Characteristic curves of the pump-turbine are displayed on **Figure 2** both in a discharge factor versus speed factor representation ( $Q_{ED}(n_{ED})$ ), and in a head coefficient

versus flow coefficient representation ( $\psi(\phi)$ ). In the following,  $D$  stands for the reference diameter of the runner ( $m$ ) and  $U$  is the peripheral velocity based on the reference diameter ( $m/s$ ).

For all the considered operating points, the deviation between the numerical and experimental head is less than 2%. This result tends to prove the ability of the numerical model to correctly predict the flow behaviour for such operating points.

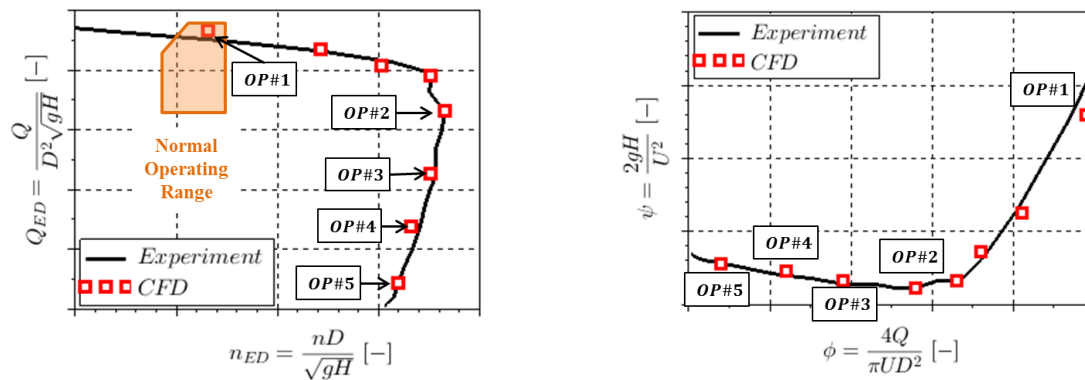


**Figure 2.** Characteristic curves of the pump-turbine – Turbine Quadrant.

The evolution of the torque with the discharge is given in **Figure 3**, in a non-dimensional form. CFD is in good agreement with the experiment, except for operating points near no load condition ( $OP\#3$  and  $OP\#4$ ). For these simulations, the torque is overestimated compared to the experimental values. This can be explained by the fact that the clearance gaps are neglected. These gaps are responsible for a leakage flow, which reduces the actual discharge passing through the runner. Furthermore, in the experimental model, the outside parts of the hub and shroud of the runner are rotating in the fluid which is inside the gaps. This fluid exerts a resisting torque on the runner, which tends to reduce the measured torque, without changing the total head.

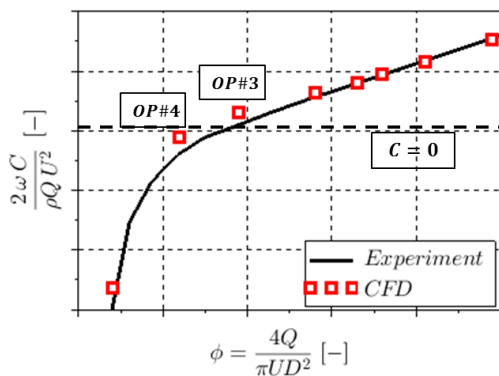


**Figure 3.** Non-dimensional torque versus discharge coefficient

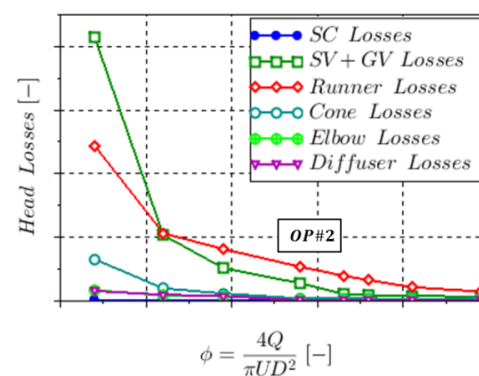


**Figure 4.** Hydraulic Losses versus discharge coefficient

Hydraulic losses in the main components of the pump-turbines are approximated by calculating the difference of mass flow averaged total pressure between the inlet and the outlet of each component taken separately. As shown on Figure 4, hydraulic losses increase with decreasing discharge. When the discharge goes below the one of  $OP\#2$ , augmentation of the losses is faster than the reduction of the torque. As a consequence, the head continues to increase between  $OP\#2$  and zero discharge, although the torque exerted on the runner becomes negative (turbine brake operation).

Hydraulic losses in the runner and in the guide vane are the most important losses. There is a high level of energy dissipation inside these two domains. When approaching the zero flowrate condition (*OP#5*), losses in the draft tube cone also increases. This shows that energy is also dissipated in the low pressure region of the pump-turbine.

### 3.2. Pressure fluctuations

**3.2.1. General Analysis.** Pressure probes are placed on the numerical model at the same locations as in the experimental setup. Four different locations are considered: inlet of the spiral casing (Probe – SC), outlet of the stay vanes (Probe – SV), the gap between the guide vane and the runner blades (Probe – Gap) and the draft tube cone (Probe – Cone). The fluctuation levels for each probe and for the different operating conditions are summarized in the **Table 2** below. Non-dimensional amplitude of fluctuation is defined as follows ( $\Delta P$  is the peak to peak value with 97% confidence of the pressure signal, in *Pa*).

$$\frac{\Delta P}{1/2 \rho U^2} \quad (2)$$

Where  $\Delta P$  is the peak-to-peak value with 97% confidence of the pressure signal (*Pa*), and  $\rho$  is the water density (*kg/m<sup>3</sup>*)

The levels predicted by CFD are in accordance with the measured levels. For off-design conditions, the pressure fluctuations are significantly higher than for *OP#1*. Maximum of fluctuation is reached for no-load conditions (*OP#3* and *OP#4*). For such operating points, the amplitude goes up to ten times the level at *OP#1*. The highest amplitude of the fluctuations occurs in the vaneless gap. Probes in the stay vanes channel and in the spiral casing have similar behaviour; except for #*OP1*, their amplitudes are about three times lower than the one in the gap. In the draft tube cone, the amplitude of pressure fluctuations is about six times lower than the one in the gap. Such behaviour tends to prove that the main sources of instabilities are located inside the vaneless gap, and that they propagate in every components of the pump-turbine. For *OP#5* the fluctuation level is around 30% lower than for the others off-design operating conditions.

**Table 2.** Pressure fluctuations (Peak to Peak 97%) at different locations inside the pump-turbine

<i>OP#</i>	Probe - SC		Probe - SV		Probe - Gap		Probe - Cone	
	Expe	Num	Expe	Num	Expe	Num	Expe	Num
<b>1</b>	0.010	0.011	0.015	0.021	0.063	0.059	0.009	0.004
<b>2</b>	0.075	0.076	0.071	0.101	0.247	0.331	0.043	0.009
<b>3</b>	0.096	0.100	0.103	0.132	0.351	0.370	0.051	0.047
<b>4</b>	0.092	0.099	0.097	0.145	0.326	0.360	0.050	0.058
<b>5</b>	0.057	0.065	0.052	0.084	0.244	0.247	0.031	0.052

**3.2.2. Spectral analysis.** Fast Fourier Transform (FFT) is applied on experimental and numerical pressure signals. Spectra for the gap and spiral casing pressure probes are displayed on **Figure 5** below. Numerical spectra exhibit some noise for the low frequencies and some peaks are less pronounced than the experimental ones. It can be explained by the fact that data acquisition for numerical computation is made during 15 to 30 runner revolutions; while 200 revolutions are considered for the experimental signals. Hence sampling error is more important for CFD. But overall, results are in good agreement with the experimental data.

For *OP#1*, the main components of the pressure fluctuations are the blade passing frequency (BPF) and its first harmonic. At the spiral casing inlet, the peak corresponding to the first harmonic has bigger amplitude than the one associated with the BPF. These oscillations are associated with Rotor-Stator Interaction (RSI) phenomena, as described by Zobeiri [9]. At off-design conditions, BPF is the main component of the pressure fluctuations in the vaneless gap, but is not visible in the spiral casing.

For *OP#4* a low frequency component peak (around 55% of the runner frequency,  $f_0$ ) with high amplitude is clearly visible **Figure 5**. This low frequency peak is dominant in the spiral casing. Sub-synchronous frequency is often associated with flow unsteadiness that may occur in pump-turbines for such operating conditions. For zero discharge conditions, some low frequency peak can be observed, but they are not the dominant frequency. Furthermore for *OP#5*, the peak associated with the BPF exhibits reduced amplitude in comparison with the other off-design conditions (25% lower). These observations tend to show that flow unsteadiness is less pronounced for *OP#5*.

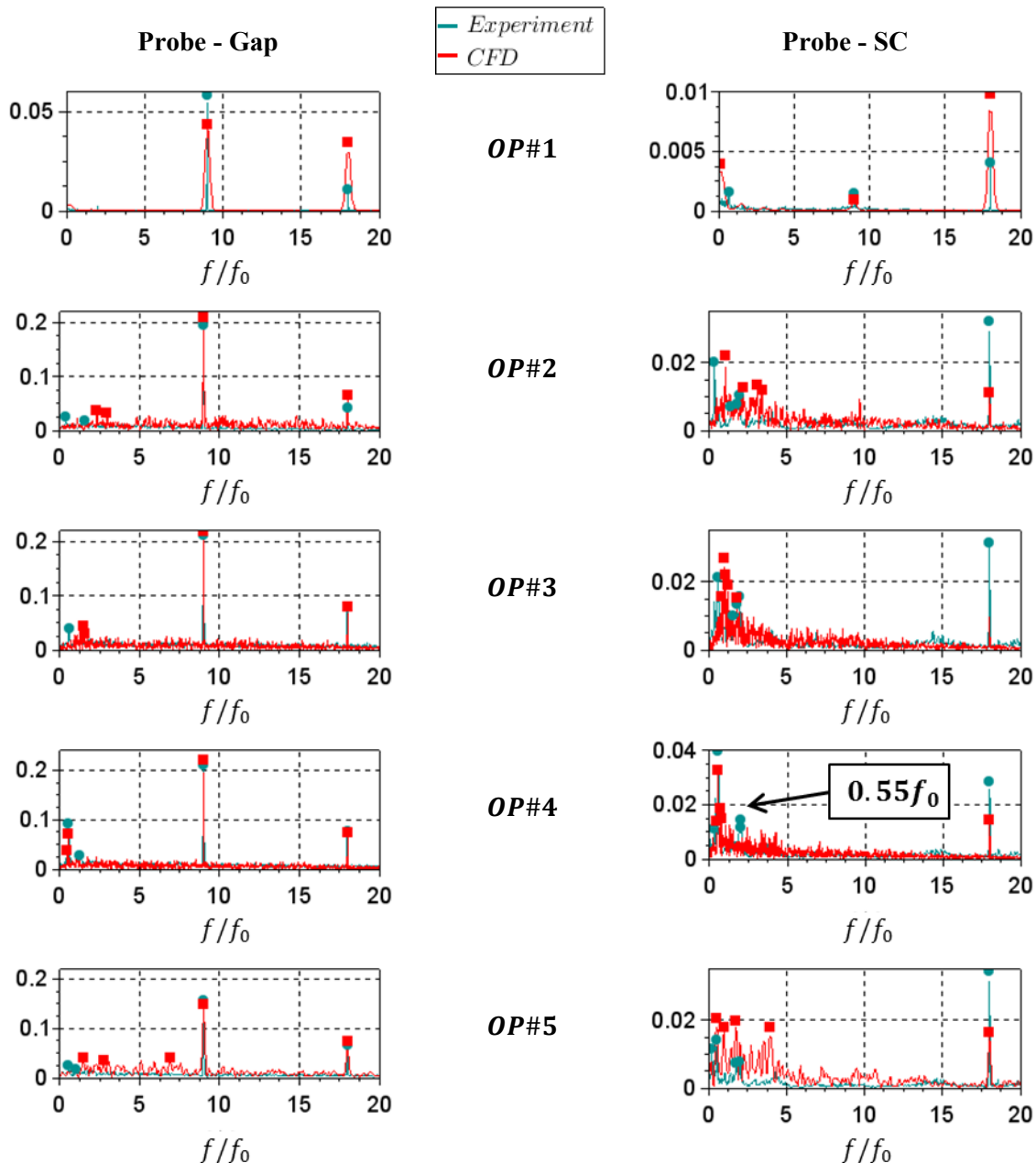


**Figure 5.** Spectra for pressure probes in the gap and in the spiral casing.

### 3.3. Study of the Blade Loadings

Time-averaged static pressure distributions along the blade length at three spanwise locations are drawn on **Figure 6** for the different discharges. Static pressure coefficient is defined as follows:

$$C_p = \frac{P - P_{inlet}}{1/2\rho U^2} \quad (3)$$

Where  $P$  is the static pressure ( $P_a$ ), and  $P_{inlet}$  is the average static pressure at runner inlet ( $P_a$ ). When the pump-turbine operates at #OP1, pressure is always higher on the pressure-side than on the suction side; except at the vicinity of the blade leading edge, due to relatively small non-zero incidence. At the blade leading edge, blade load is almost evenly distributed over the blade height. While at the trailing edge, blade load seems to be more important near the shroud.

For *OP#2* the blade load becomes negative between the leading edge and about 30% of the blade chord. Negative blade load implies that hydraulic angle at the runner inlet is significantly smaller than the geometrical angle of the blade. Blade load for the rest of the blade length is positive, but it is significantly reduced in comparison with *OP#1*. For *OP#3* and *OP#4*, blade loads at the leading edge are relatively similar to the one for *OP#2*, showing negative values. The static pressure on the pressure side is reduced, causing lower blade load. Thus, no-load condition seems to show an equilibrium between negative and positive blade loads, as described by Liang and Keller [5].

At zero flow-rate condition, overpressure at entrance of the blade seems to be reduced and negative blade load region covers only 20 percent of the blade chord. Pressure difference between pressure and suction sides is drastically reduced compared with the other operating conditions. Hence the torque exerted on the runner goes to significant negative value for *OP#5*.

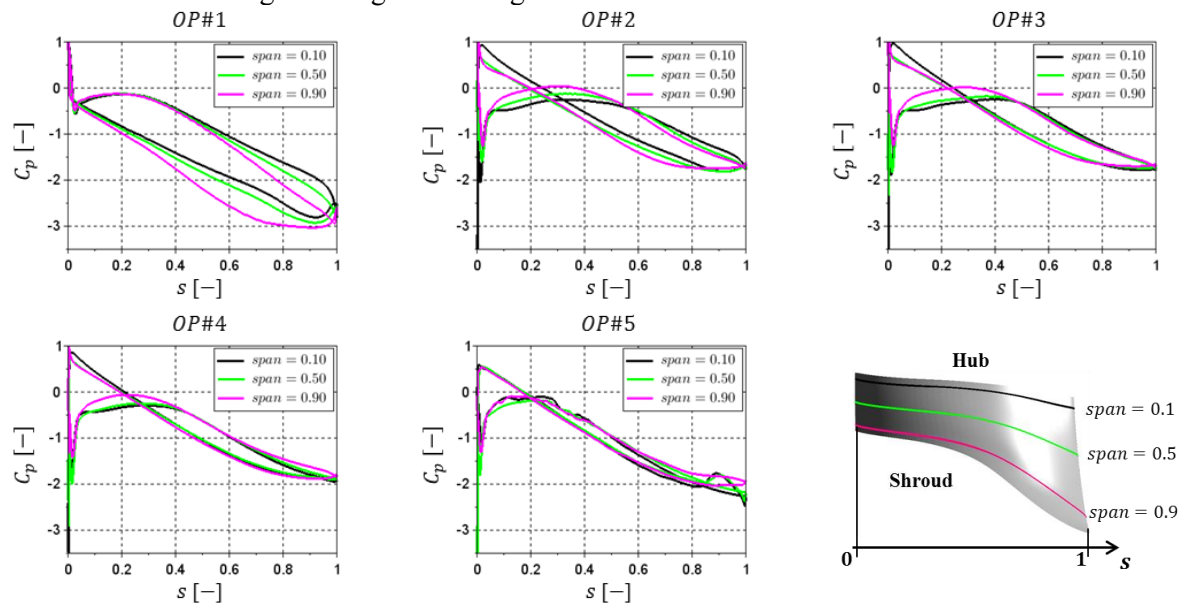


**Figure 6.** Blade loadings at three different spanwise locations

### 3.4. Study of the flow patterns at runner inlet

Time and circumferentially averaged radial and circumferential velocity profiles at runner inlet are displayed on **Figure 7** and **Figure 8**, respectively. Profiles for *OP#1* are relatively uniform over the channel height. While for *OP#2* and lower discharges, profiles exhibit strong gradients. Furthermore, negative value for the discharge velocity indicates a backflow in the guide vanes domain. Position of this backflow depends on the considered operating point. For *OP#2* to *OP#4* negative velocity region is located in the upper part of the channel near the hub. Whereas for *OP#5*, backflow covers a large part of the channel around mid-span, and inflow regions are confined near the hub and shroud sides.



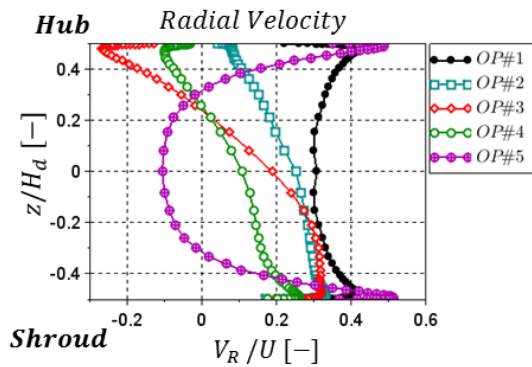


**Figure 7.** Time-averaged discharge velocity profile at runner Inlet

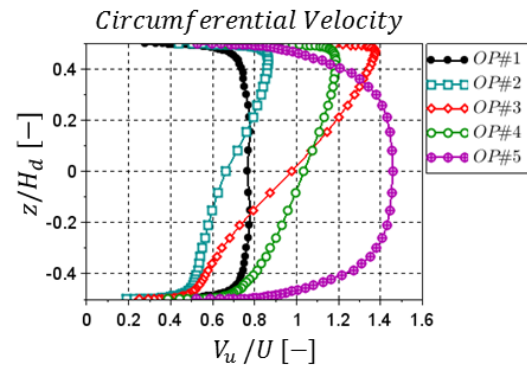


**Figure 8.** Time-averaged circumferential velocity profile at runner inlet

Backflow regions are associated with higher circumferential velocity than the inflow regions. Hence, the fluid exits the runner with an increased level of kinetic energy. This confirms that the runner partially acts as a pump and transfers energy back to the fluid. The flow is mainly in the turbine direction, the backflow has then to eventually re-enter in the runner domain. As described by Staubli et al. [4], such roll-up of the backflow leads to the formation of helical vortices that develop in the vaneless space between the guide vane and the runner and partially block the main flow. Blockage effect induced by the vortices can be clearly evidenced by looking at the streamlines of meridian velocity on **Figure 9**. Interactions between the high kinetic energy vortices, the runner blades and the inflow coming from the guide vane channels are highly turbulent and induce a large amount of energy dissipation. Hence, the total head of the pump-turbine increases due to these losses.

The flow pattern for *OP#5* is quite different. Two counter rotating vortices are present in the vaneless gap. Blockage effect is more important than for the other operating conditions. The fluid enters the runner at hub and shroud side and flows back at the middle of the meridian channel. Such flow features have already been observed for smaller guide vane opening by Widmer et al. [10].

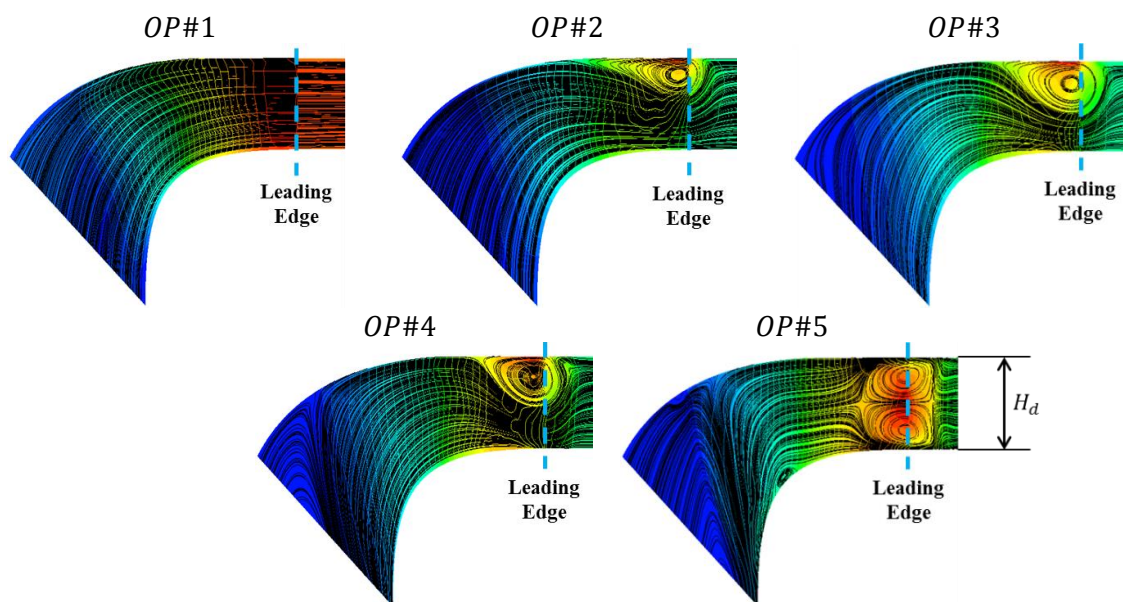


**Figure 9.** Streamlines of meridian velocity coloured by of the total pressure along the meridian channel (time and circumferentially averaged values).



### 3.5. Rotating stall evidence

Even though generally found in compressors or pumps at part load [11], it is now well established that Rotating Stall (RS) may occur in pump-turbines operating in turbine brake region [10], [12], [13]. For *OP#4*, spectral analysis of the pressure fluctuations has revealed a peak associated with high amplitude for approximately 55% of the runner frequency (**Figure 5**). This low frequency component is also clearly visible when analysing the torque on the guide vanes. Considering the torque applied on a single runner blade, a peak is observed for 45% of the runner frequency. This difference between the frequency measured in the rotating and absolute frames indicates that this instability is due to the presence of one structure rotating at 55% of the rotation speed of the runner.

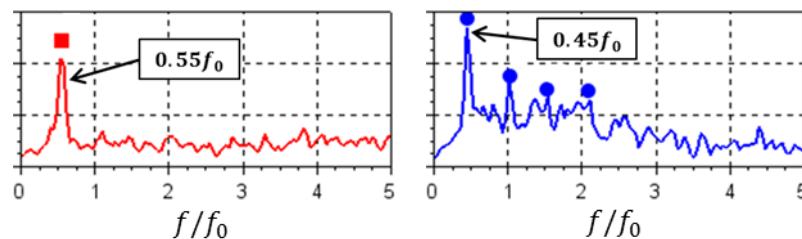


**Figure 10.** Spectra for torque on a guide vane (left) and on a runner blade (right), for *OP#4*

Instantaneous streamlines for two distinct simulation times are displayed on **Figure 11**. For the first simulation time (left side of the picture) flow is stalled in the guide vanes channel located near the spiral casing tongue (upper side) and the discharge in the corresponding stay vane channel is reduced. Discharge in the other channels is increased, to ensure conservation of the total discharge. Reverse observations can be done for the second simulation time (right side of the picture), where non-stalled flow is present in the channel near spiral casing tongue. These observations corroborate the existence of one rotating stall cell that spans over approximately ten guide vane channel. Stalled flow induces blockage effect and forces redistribution of the discharge upstream of the stay vanes channels. Relative rotor/stator position seems to have a small influence on the redistribution of the discharge.

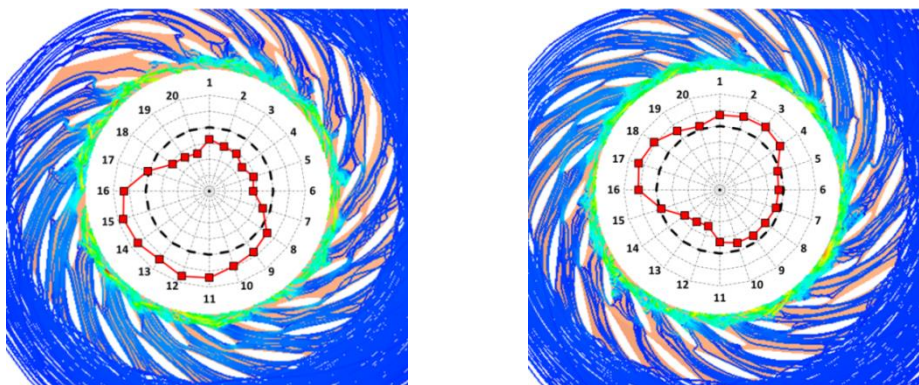


**Figure 11.** Instantaneous streamlines in the stay vanes and guide vanes channel, coupled with instantaneous discharge through the stay vane channels (represented in the figure centre), for two simulation times (*OP#4*). Homogeneous discharge distribution is indicated by the black dotted line.

## 4. Conclusions

Unsteady numerical simulations were performed on a full model scale pump-turbine for operating condition varying from optimal efficiency point to zero flow-rate conditions, for a given large guide vane opening. The good match between experiment and CFD results has shown the ability of the SAS-

SST turbulence model to accurately predict the flow behaviour inside the pump-turbine, for a wide range of operating conditions.

Spectral analysis of the pressure signals showed that for off-design conditions, fluctuations greatly increase compare to *OP#1*. The main source of unsteadiness is located in the vaneless gap between the guide vanes and the runner. The study of the flow patterns underlined the fact that the “S-shaped” of the characteristic is linked to the onset of a backflow in the vaneless space between the guide vane and the runner. This backflow is due to flow separation in the inter-blade channels. The increasing size and intensity of the backflow with the decreasing discharge lead to larger blockage effect and higher momentum exchange between the backflow and the flow coming from the guide vanes; causing higher energy dissipation. Rotating stall developing in the guide vanes channels has been identified for operating condition in turbine brake region, but it is not the main reason for the S-shape of the characteristic.

The geometry considered in the present paper is an usual geometry for pump-turbine in GE Hydro. Which gives confidence in the fact that observed phenomena are common in pump-turbines at off-design conditions. The current methodology for estimation of the S-shape will be applied on more recent runner geometries in order to improve the comprehension of these phenomena.

## References

- [1] T. Staubli, F. Senn, and M. Sallaberger, 2008, ‘Instability of pump-turbines during start-up in the turbine mode’, *Hydro2008 Ljubl. Slov. Pap.*, no. 9.6.
- [2] S. Pejovic, L. Krsmanovic, R. Jemcov, and P. Crnkovic, 1976, ‘Unstable operation of high-head reversible Pump-Turbines’, Leningrad.
- [3] C. Nicolet, S. Alligné, B. Kawkabani, J.-J. Simond, and F. Avellan, 2009, ‘Unstable operation of Francis pump-turbine at runaway: rigid and elastic water column oscillation modes’, *Int. J. Fluid Mach. Syst.*, vol. 2, no. 4, pp. 324–333.
- [4] T. Staubli, C. Widmer, T. Tresch, and M. Sallaberger, 2010, ‘Starting pump-turbines with unstable characteristics’, *Hydro 2010*.
- [5] Q. Liang and M. Keller, 2010, ‘Behavior of pump turbines operating at speed no load condition in turbine mode’, *Hydro Vis.*.
- [6] G. Olimstad, T. Nielsen, and B. Børresen, 2012, ‘Dependency on Runner Geometry for Reversible-Pump Turbine Characteristics in Turbine Mode of Operation’, *J. Fluids Eng.*, vol. 134, no. 12, p. 121102, 2012.
- [7] F. R. Menter and Y. Egorov, 2010, ‘The Scale-Adaptive Simulation Method for Unsteady Turbulent Flow Predictions. Part 1: Theory and Model Description’, *Flow Turbul. Combust.*, vol. 85, no. 1, pp. 113–138.
- [8] F. R. Menter, 2012, ‘Best practice: Scale-resolving simulations in ANSYS CFD’, *ANSYS Ger. GmbH*, pp. 1–70.
- [9] A. Zobeiri, J.-L. Kueny, M. Farhat, and F. Avellan, 2006, ‘Pump-turbine rotor-stator interactions in generating mode: Pressure fluctuation in distributor channel’, in *23rd IAHR Symposium on Hydraulic Machinery and Systems*.
- [10] C. Widmer, T. Staubli, and N. Ledergerber, 2011, ‘Unstable characteristics and rotating stall in turbine brake operation of pump-turbines’, *J. Fluids Eng.*, vol. 133, no. 4, p. 041101.
- [11] O. Pacot, C. Kato, Y. Guo, Y. Yamade, and F. Avellan, 2016, ‘Large Eddy Simulation of the Rotating Stall in a Pump-Turbine Operated in Pumping Mode at a Part-load Condition’, *J. Fluids Eng.*.
- [12] V. Hasmatuchi, M. Farhat, S. Roth, F. Botero, and F. Avellan, 2011, ‘Experimental evidence of rotating stall in a pump-turbine at off-design conditions in generating mode’, *J. Fluids Eng.*, vol. 133, no. 5, p. 051104.
- [13] G. Cavazzini, A. Covi, G. Pavesi, and G. Ardizzone, 2016, ‘Analysis of the unstable behavior of a pump-turbine in turbine mode: fluid-dynamical and spectral characterization of the S-Shape characteristic’, *J. Fluids Eng.*, vol. 138, no. 2, p. 021105.